Journal of Nuclear Materials 399 (2010) 108–113

Contents lists available at ScienceDirect

Journal of Nuclear Materials

journal homepage: www.elsevier.com/locate/jnucmat

The dependence of carbide morphology on grain boundary character in the highly twinned Alloy 690

Hui Li, Shuang Xia *, Bangxin Zhou, Wenjue Chen, Changliang Hu

Institute of Materials, Shanghai University, Shanghai 20072, PR China

ARTICLE INFO

Article history:
Received 11 July 2009
Accepted 12 January 2010

ABSTRACT

The dependence of morphology of grain boundary carbides on grain boundary character in Alloy 690 (Ni–30Cr–10Fe, mass fraction, %) with high fraction of low Σ coincidence site lattice (CSL) grain boundaries was investigated by scanning electron microscopy (SEM) and transmission electron microscopy (TEM). Some of the surface grains were removed by means of deep etching. It was observed that carbides grow dendritically at grain boundaries. The carbide bars observed near incoherent twin boundaries and twin related Σ9 grain boundaries are actually secondary dendrites of the carbides on these boundaries. Higher order dendrites could be observed on random grain boundaries, however, no bar-like dendrites were observed near Σ27 grain boundaries and random grain boundaries. The morphology difference of carbides precipitated at grain boundaries with different characters is discussed based on the experimental results in this paper.

1. Introduction

The nickel based Alloy 690 (Ni–30Cr–10Fe, mass fraction, %) which has superior resistance to intergranular stress corrosion cracking (IGSCC) and intergranular corrosion (IGC) in various environments [1–4] has been used as a steam generator tube material in pressurized water reactor (PWR) of nuclear power plants. Although the steam generator tubes made of Alloy 690 have good performance, prolonged service life and improved performance of steam generator tube material have been highly demanded by nuclear energy industry.

The morphology of grain boundary carbides has been extensively studied in face center cubic (FCC) structure Fe–Cr–Ni alloys [4–14], because grain boundary carbide precipitation has strong influence on the resistance to intergranular failures [11,15–20]. Many studies [5,8,10,14,21] showed that the grain boundary misorientation can strongly affect the precipitation of chromium-rich carbide. Low Σ ($\Sigma \leqslant 29$) coincidence site lattice (CSL) grain boundaries have lower susceptibilities to carbide precipitation than random grain boundaries [10,22–24]. Almost all of the reports [5–10,13,14,21] about carbide morphology in austenitic stainless steels and Alloy 690 showed that the morphology of carbides precipitated at twin boundaries is distinct from that precipitated at random grain boundaries. They showed that the plate-like carbide precipitates can often be observed at the incoherent twin boundaries, while there is no such kind of carbide at other type boundaries. However, it is not clear why the carbide morphology is different at grain boundaries with different characters so far.

In this paper, the proportion of twin related low ΣCSL grain boundaries was increased by grain boundary engineering (GBE). After that, there were many twin related grain boundaries available for study. Morphology of carbides precipitated at grain boundaries with different characters was investigated. In order to study the three dimensional morphology of carbide, deep etching method was used. The reason for the carbide morphology differences at grain boundaries with different characters was discussed, combined with the TEM observations.

2. Experimental procedures

The chemical composition of the investigated Alloy 690 is given in Table 1. The specimens were solution annealed at 1100 °C for 15 min, and then quenched into water (WQ). The 10% cold rolling and subsequent recrystallization annealing at 1100 °C for 5 min and WQ were employed as thermomechanical processing (TMP) of GBE [25]. This TMP not only increased the proportion of twin related low ΣCSL grain boundaries to more than 70%, but also resulted in a solution annealed state. The mechanism involved in the GBE was discussed by Xia et al. elsewhere [26,27]. The aging treatments were carried out at 715 °C for different time to cause carbide precipitation at grain boundaries.

Prior to the scanning electron microscopy (SEM) and the electron backscatter diffraction (EBSD) experiments, the electro-polishing was carried out in a solution of 20% $HClO_4$ + 80% CH_3COOH at room temperature with 30 V direct current for 30 s. Electro-etching was carried out in the same solution with 5 V direct

* Corresponding author. Tel.: +86 13817106410.
E-mail addresses: xiashuang14@sohu.com, xs@shu.edu.cn (S. Xia).

0022-3115/$ - see front matter © 2010 Elsevier B.V. All rights reserved.
doi:10.1016/j.jnucmat.2010.01.008

Table 1
The chemical composition of the investigated Alloy 690 (mass fraction, %).

Ni	Cr	Fe	C	N	Ti	Al	Si
60.52	28.91	9.45	0.025	0.008	0.4	0.34	0.14

current for 5 s. EBSD was employed to determine the grain boundary misorientation using the TSL laboratories orientation imaging microscopy (OIM) system attached to a Hitachi S-570 SEM. The characters of grain boundaries were classified according to the Palumbo–Aust criterion [28]. The specimens were examined in a JSM-6700F SEM operated at 15 kV to study the carbide morphology at grain boundaries with different characters.

After EBSD examination, some specimens were deeply etched in a solution of 65% HNO_3 + 0.2% HF + 34.8% H_2O for 92 h at room temperature to remove some of the surface grains. After that the carbides on the grain boundary surface were observed by SEM.

Transmission electron microscopy (TEM) thin specimens were prepared by twin jet electro-polishing in a solution of 20% $HClO_4$ + 80% CH_3COOH with 30 V direct current at room temperature. TEM observations were conducted with JEM 2010F TEM operated at 200 kV. The misorientation of grain boundary was determined by selected area electron diffraction (SAD) on both sides of that grain boundary.

3. Results and discussion

3.1. Identification of grain boundary carbides

Fig. 1a and b shows the bright-field and dark-field TEM images of grain boundary carbides, respectively. Fig. 1c shows the indexed SAD pattern of a carbide particle in Fig. 1a. In Fig. 1c, the *m* represents matrix and *c* carbide. It can be seen from Fig. 1c that the carbide was identified as $M_{23}C_6$ with an FCC crystal structure and a lattice parameter of $a_c \sim 1.06$ nm. This type of carbide on grain boundary has a cube-to-cube orientation relationship to one side of the matrix (lattice parameter $a_m \sim 0.35$ nm).

3.2. The dependence of carbide morphology on grain boundary character

EBSD technique was used to identify the grain boundary character. Fig. 2 shows the dependence of carbide morphology on grain boundary character. Fig. 2a indicated that the grain boundary character distribution (GBCD) of the specimens aged at 715 °C for 15 h after TMP is similar to that of the specimens only treated by TMP as described in our previous work [29]. The TMP parameters used in this study and previous study [29] are as follows: 10% cold rolling and subsequent recrystallization annealing at 1100 °C for 5 min and WQ. The GBCD statistics of specimens before and after aging treatment are similar (Fig. 3), and Downey et al. [30] reported that the grain boundary character in 316 austenitic stainless steel was stable after aging at 700 °C for 1–100 h. So it is clear that carbides are forming on a statistically relevant stable set of grain boundaries.

The annealing twins have a Σ3 misorientation with its parent orientation (Fig. 2a). Σ3 boundaries can be classified as coherent twin boundary and incoherent twin boundary. Fig. 2b gives the morphology of carbides precipitated at Σ3 boundaries. The carbides precipitated near incoherent twin boundary are plate-like, which is consistent with the study in other literatures [9,13,14]. In contrast to the plate-like carbides precipitated near the incoherent twin boundary, the tiny carbide particles distribute densely on that incoherent twin boundary (Fig. 2b). Because of the ordered atomic arrangement, the interface energy of coherent twin boundary is very low. Only a few plate-like carbides can be found on coherent twin boundary under the present experimental condition (Fig. 2b). The carbide morphology and distribution are different between precipitated at coherent twin boundary and precipitated at incoherent twin boundary. This difference indicates that the inclination of grain boundary plane influence the morphology of carbides significantly.

Fig. 2c shows the morphology of carbides precipitated at a twin related Σ9 grain boundary. The carbide morphology near Σ9 grain boundary in Fig. 2c is plate-like, and similar to that at the incoherent twin boundary. However, the carbide plates grow from the grain boundary into only one side matrix of that Σ9 grain boundary (Fig. 2c). Some continuous carbide particles which are a little bigger than that precipitated on incoherent twin boundary also distribute on that Σ9 grain boundary (Fig. 2c). As shown in Fig. 2b and c, carbides precipitated at both incoherent Σ3 boundary and Σ9 grain boundary are plate-like, and therefore they may grow in the same manner.

The morphology of carbides precipitated on Σ27 grain boundary and on random grain boundary are given in Fig. 2d and e, respectively. No specific shapes of the carbides are revealed in Fig. 2d and e. The sizes of carbides precipitated on Σ27 grain boundary and on random grain boundary are much bigger than those precipitated on Σ3 and Σ9 grain boundaries due to the

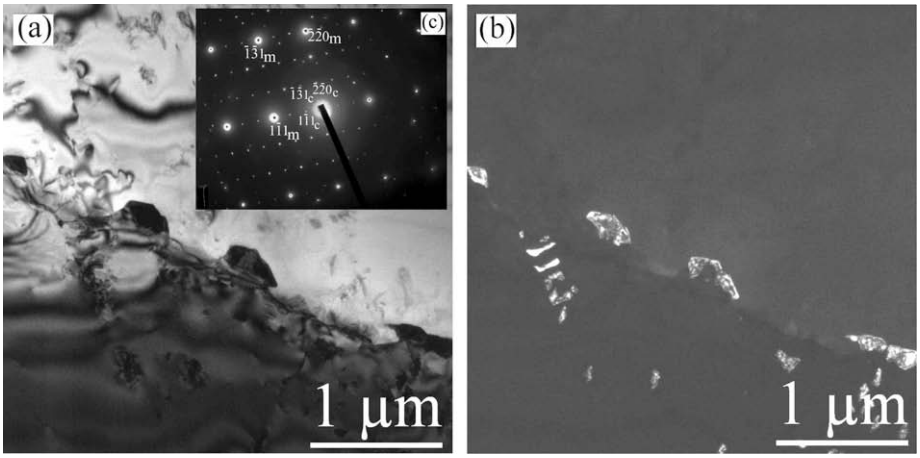

Fig. 1. The identification of $M_{23}C_6$ precipitated on grain boundary in Alloy 690 aged at 715 °C for 15 h after TMP, bright-field TEM image (a), dark-field TEM image (b), indexed select area electron diffraction pattern (c).

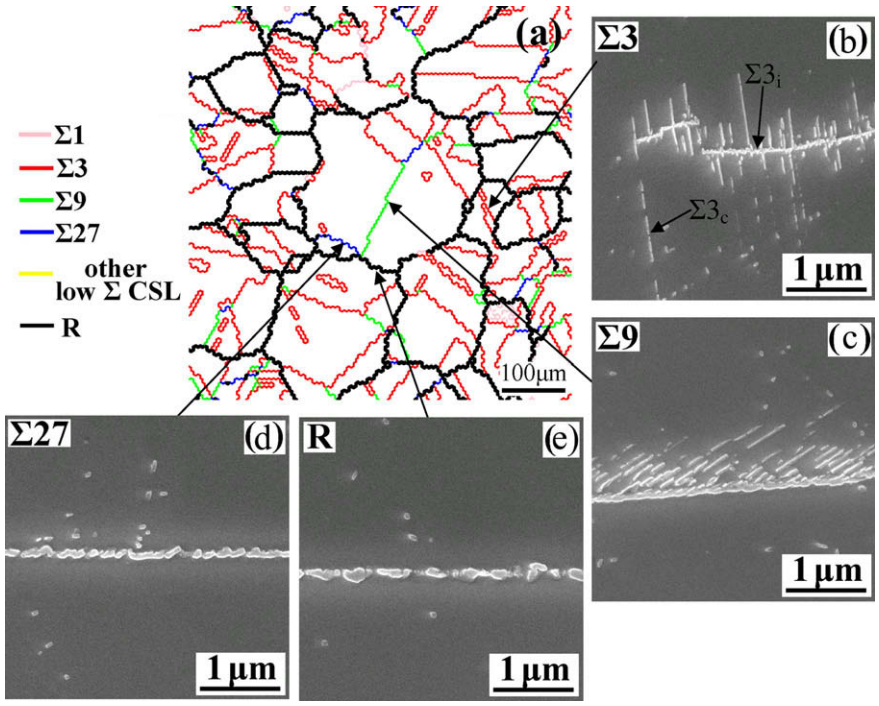

Fig. 2. Dependence of carbide morphology on grain boundary characters in the specimens aged at 715 °C for 15 h after thermomechanical process. OIM map of the observed specimen (a), morphology of carbides precipitated at Σ3 grain boundary (b), at Σ9 grain boundary (c), at Σ27 grain boundary (d), and at random grain boundary (e). $\Sigma3_i$: incoherent twin boundary, $\Sigma3_c$: coherent twin boundary, *R*: random grain boundaries.

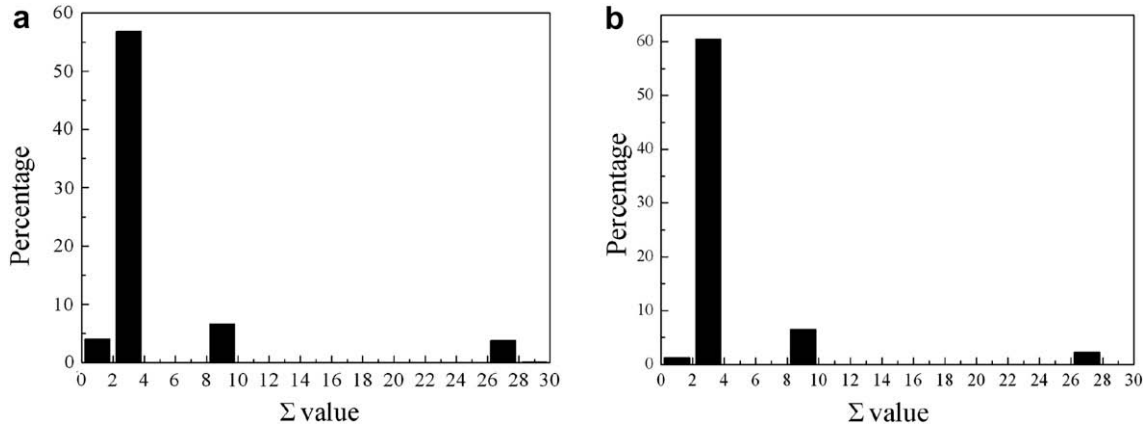

Fig. 3. Grain boundary character distribution statistics of the TMP specimens before (a) [28] and after (b) aging treatment.

higher interface energy (Fig. 2). It can be clearly seen that there are no plate-like carbides near Σ27 grain boundary and random grain boundary.

3.3. The reason for various carbide morphology characteristics at grain boundaries with different characters

3.3.1. The actual morphology of grain boundary carbides

In order to obtain more information about the morphology of grain boundary carbides, some specimens were deeply etched to remove some grains on the specimen surface. After deep etching, the three dimensional morphology of grain boundary carbides can be revealed.

Fig. 4 gives the morphology of carbides precipitated at grain boundaries after deep etching. All of the carbides grow dendritically on the random grain boundary plane. Secondary dendrites grow on primary dendrite, and sometimes higher order dendrites can form on secondary dendrite (Fig. 4a and b). From the three dimensional observation (Fig. 4c and d), it can be seen that all of the carbides near incoherent twin boundary and twin related Σ9 grain boundary are bar-like rather than plate-like as predicted in other literatures [5,6,9,30]. The different descriptions of the carbide morphology are caused by the different appearances between two dimensional and three dimensional observations.

The dendrite morphology formation may be associated with the segregation and concentration changes of chromium and carbon at the outer regions of the dendrites during $M_{23}C_6$ growth. The good matching crystallographic direction between the matrix and $M_{23}C_6$ is the ⟨1 1 0⟩ directions on {1 1 1} planes [5,31]. Therefore the chromium-rich $M_{23}C_6$ grows in the ⟨110⟩ direction on {1 1 1} plane. However, the growth of carbide would consume carbon and chromium ahead of the moving interface between carbide and matrix. When the concentration of carbon and chromium decrease to the extent that cannot afford further growth in the original direction,

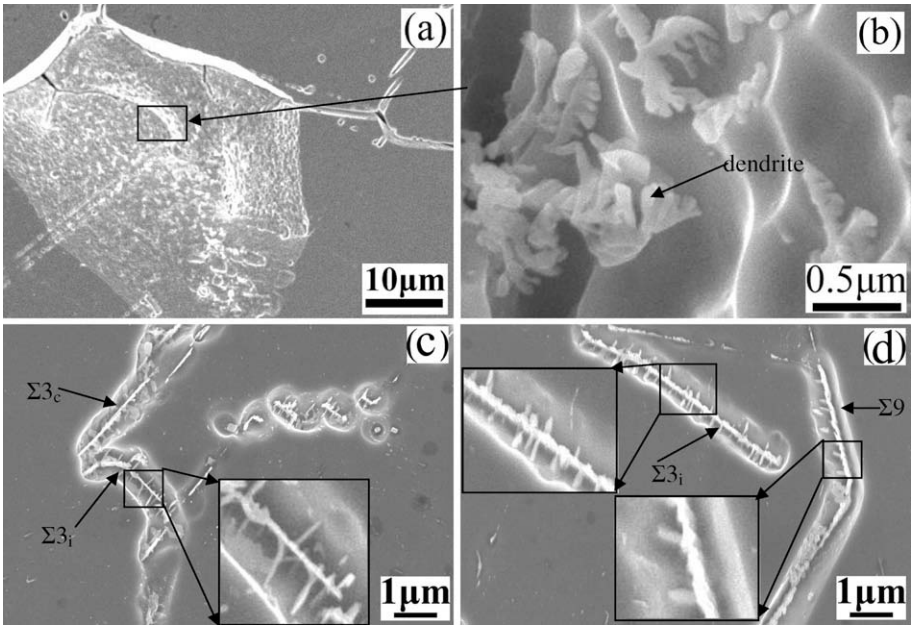

Fig. 4. Carbide morphology observed after deep etching, image of deeply etched specimen (a), the morphology of carbides precipitated at random grain boundary (b), at incoherent twin boundary (c), and at Σ9 grain boundary (d). $\Sigma 3_i$, incoherent twin boundary; $\Sigma 3_c$, coherent twin boundary.

the dendrites will initiate along another ⟨1 1 0⟩ direction on {1 1 1} plane which have higher chromium concentration. Hence, we believe that all the $M_{23}C_6$ grow dendritically at grain boundaries in the current experimental condition.

3.3.2. The morphology of carbides precipitated at incoherent twin boundary and Σ9 grain boundary

As shown in Section 3.2, morphology of carbides precipitated at both incoherent Σ3 boundary and Σ9 grain boundary are similar, and therefore they may grow in the same manner. There are several mechanisms to explain the bar-like carbides formation near incoherent twin boundary [5,6,9,29]. Beckitt and Clark [6] suggested that $M_{23}C_6$ particles nucleated at boundary, and then the dislocations move out from an incoherent twin boundary under a stress generated by the growth of carbides and continue to act as nucleating sites for further precipitation. However, if $M_{23}C_6$ bars could form by the repeated nucleation on a migrating dislocation, such bars might have been commonly observed elsewhere in the matrix, because $M_{23}C_6$ also nucleate on dislocations inside grains. According to the work of Singhal and Martin [31], stacking faults are created by the gliding of dislocations from the incoherent twin boundary. $M_{23}C_6$ grows across the faults forming bars. The subsequent growth of a bar, according to them, occurs as the partial dislocation glides further, and the precipitation process is repeated. Lewis and Hattersley [5] have ruled out the possibility of precipitation of $M_{23}C_6$ *via* this stacking fault. Sasmal [9] suggest that the residual stress localized on either side of an incoherent twin boundary is tensile in nature and of a higher magnitude compared to other regions of a grain. Nucleation of $M_{23}C_6$ bars with only one habit (i.e., the twinning plane) instead of possible other {1 1 1} planes and their growth in a specific direction are influenced by the specific stress field developed in these regions, which is governed by the crystallography and geometry of a particular twin and the elastic anisotropy of the matrix. If the growth of $M_{23}C_6$ is influenced by this stress field, however, such plates might have been frequently observed near random grain boundaries where the stress field might also exist. In fact, bar-like $M_{23}C_6$ are not commonly observed near random grain boundaries.

The mechanisms discussed above are incompatible with each other. And all of these mechanisms are based on the two dimensional observations. There are some disadvantages to explain the morphology of carbides based on two dimensional cross section observations.

As shown previously, the bar-like carbides near incoherent twin boundary and twin related Σ9 grain boundary are the secondary dendrites initiated from the primary dendrite carbides precipitated on those incoherent twin boundary and twin related Σ9 grain boundary (Fig. 4c and d). Because of the low interface energy of incoherent twin boundary and twin related Σ9 grain boundary, the carbide dendrites grow not only on grain boundary, but also into the sideward matrix. The bar-like carbide dendrites grow with axes parallel to the ⟨1 1 0⟩ directions on {1 1 1} planes due to the good matching in the ⟨1 1 0⟩ directions on {1 1 1} planes between the matrix and $M_{23}C_6$ [5,31]. One nature of dendrites is that the growth directions of the same order dendrites are parallel to each other, so the carbide bars are parallel to each other (Figs. 2b and c, 4c and d).

Most observations of other people's work showed that the carbide bars do not commonly connect with the incoherent twin boundary [5–9,14,31]. This is a misunderstanding due to the two dimensional observations. This can be explained schematically by Fig. 5. Most of the observations of Refs. [5–9,14,31] are in two dimensional cross section of the carbide structure. If the observation cross section is parallel to the carbide bar as shown by plane 1 in Fig. 5a, one can see that the carbide bars connect with the interface of incoherent twin boundary as shown in Fig. 5b. However, if the cross section is not parallel to the carbide bar as shown by plane 2 in Fig. 5a, the false appearance that carbide bars do not connect with the interface of incoherent twin boundary is revealed as shown in Fig. 5c.

The main difference of carbide morphology between incoherent twin boundary and twin related Σ9 grain boundary is that carbide bars precipitated near both sides of incoherent twin boundary, while carbide bars precipitated near only one side of Σ9 grain boundary. The best matching planes between $M_{23}C_6$ and the matrix is $\{1\,1\,1\}_d//\{1\,1\,1\}_m$ [5,31]. So carbide particles initiate to nucleate on grain boundaries and have $\{1\,1\,1\}_c//\{1\,1\,1\}_m$ coherent

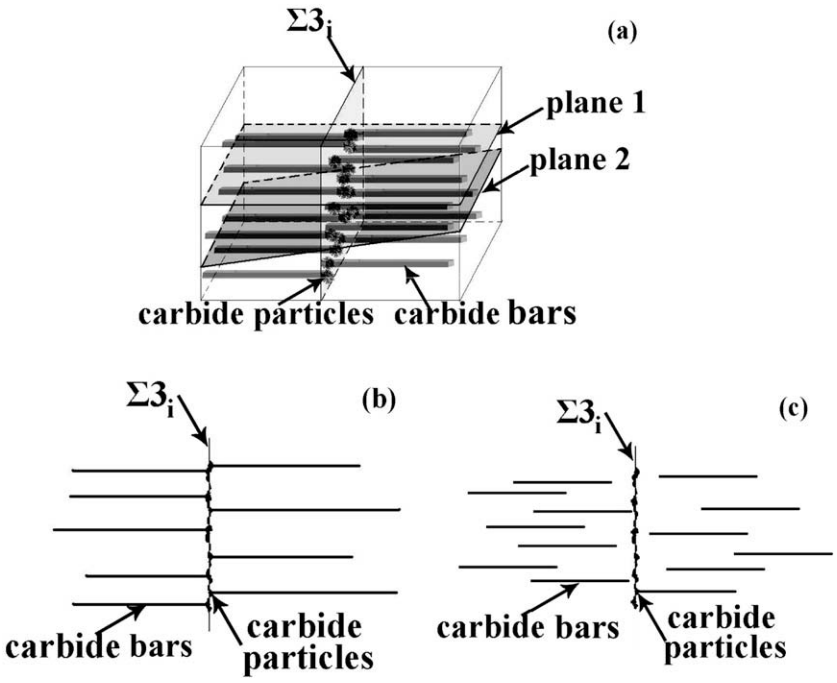

Fig. 5. Schematic illustration of the carbide morphology observed on different cross sections with the same carbides precipitated at incoherent twin boundary: (a) the three dimensional morphology of the carbides, (b) cross section view of the plane 1 in (a), (c) cross section view of the plane 2 in (a).

orientation relationship with one side of the matrix. Because the misorientation of Σ3 boundary is ⟨1 1 1⟩/60°, one of the {1 1 1} planes in one side of boundary are parallel to one of the {1 1 1} planes in the other side of that boundary, as can be illustrated by Fig. 6. Fig. 6a and b give the comparison of bright-field TEM image and dark-field TEM image of carbides precipitated at incoherent twin boundary. From Fig. 6c, which gives the corresponding SAD of Fig. 6a, one can see that the bar-like carbides are coherent with the grains in both sides of the incoherent twin boundary, and the carbide bars grow along $\langle 1\ 1\ 0\rangle_m$. From Fig. 6b, it can be concluded that all the carbide particles and bars near incoherent twin boundary grow with the same crystal orientation. So, the dendritic carbide bars can grow into the matrix near both sides of Σ3 incoherent boundary and maintain the coherent orientation relationship with nearby matrix. The misorientation of Σ9 grain boundary is ⟨1 1 0⟩/38.9°, one of the {1 1 1} planes in one side of boundary generally do not parallel to one of the {1 1 1} planes in the other side of boundary. So, the dendritic carbide bars grow into the matrix near only one side of Σ9 grain boundary which has $\{1\ 1\ 1\}_c$ //$\{1\ 1\ 1\}_m$ coherent orientation relationship with the matrix.

3.3.3. Morphology of carbides precipitated at Σ27 and random grain boundaries

If the interface energy of the grain boundary is high, the carbide dendrites grow on the grain boundary easily, and they do not penetrate into the matrix. Therefore, the carbide particles can be observed only on grain boundaries rather than grow into the nearby matrix, as shown in Fig. 2d and e.

Fig. 7 schematically illustrates the carbide morphology observed on different cross sections of the same carbide precipitated at random grain boundary. Fig. 7a shows a three dimensional

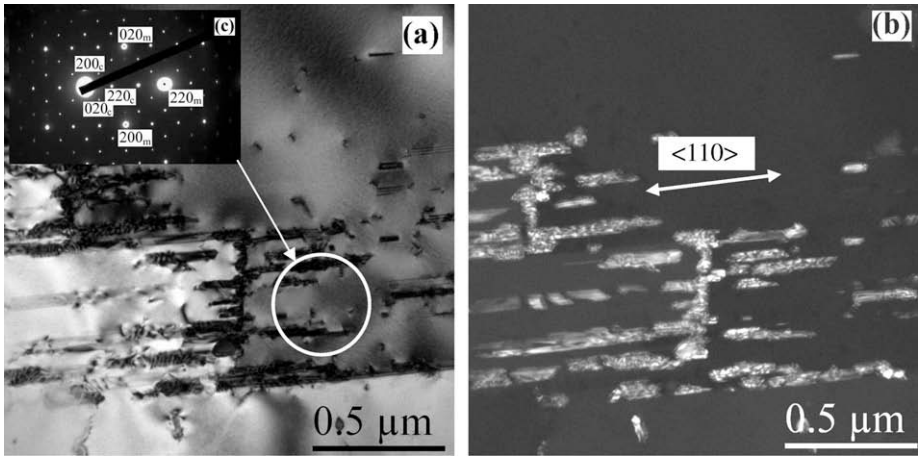

Fig. 6. TEM images of the specimens aged at 715 °C for 15 h after TMP, bright-field TEM image (a) and dark-field TEM image (b) of carbides precipitated at incoherent twin boundary, indexed select area electron diffraction pattern (c).

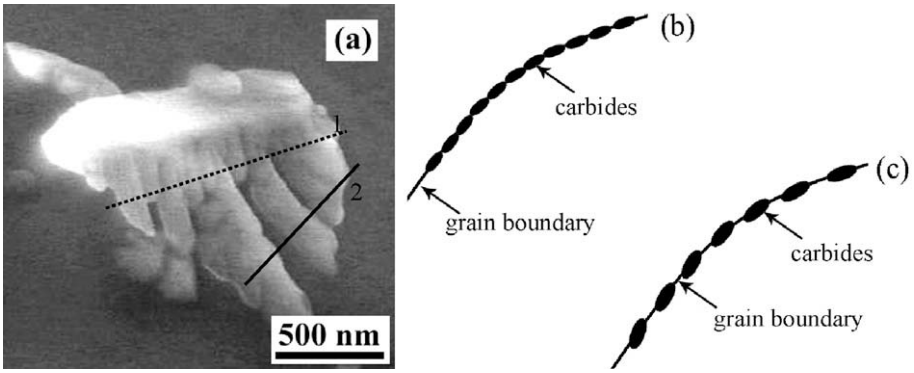

Fig. 7. Schematic illustration of the carbide morphology observed on different cross sections with same dendritic carbide precipitated on random grain boundary. (a) The three dimensional morphology of the dendritic carbide, (b) cross section view of the plane 1 in (a), (c) cross section view of the plane 2 in (a).

morphology of a dendritic carbide precipitated on random grain boundary. If the cross section is the plane 1 in Fig. 7a, the observed carbides are small and continuous. However, if the cross section is the plane 2 in Fig. 7a, the observed carbides are large and discrete. Therefore the morphology of carbides depended more on the observing cross section beside the actual shape of the carbides. So it is general observed that the morphology of carbides precipitated at Σ27 grain boundary and random grain boundary do not have specific geometry shapes. This is the reason why the generally observed morphology of carbides did not have specific geometry shapes. From the observations and discussions above, we believe that all the grain boundary carbides grow dendritically. The interface energy of grain boundary can influence carbide shape, size and distribution. The observed morphology of carbides precipitated at grain boundary generally depends on the observing cross section. Three dimensional observation is necessary when study microstructures in materials.

4. Conclusions

Based on the experimental results and discussions above, the following conclusions can be drawn:

(1) Carbide precipitated near incoherent twin boundary and twin related Σ9 grain boundary is bar-like rather than plate-like.
(2) Carbides grow dendritically at grain boundaries despite the boundary characters. The bar-like carbides near incoherent twin boundary and twin related Σ9 grain boundary are actually secondary dendrites of the carbides on these boundaries. The higher order dendrites can be observed on random grain boundary.
(3) The bar-like carbide grows near both sides of incoherent Σ3 boundary, while near only one side of Σ9 grain boundary. No bar-like carbide can be observed near Σ27 grain boundary and random grain boundary.
(4) The observed morphology of carbides precipitated at grain boundary generally depends on the observing cross section. When it is observed on different cross sections, the same carbide may show different morphologies.

Acknowledgements

The authors would like to thank Prof. S.J. Zhao for reading and polishing the English usage of the manuscript, and would like to thank Mr. Y.L. Chu and Mr. Q.D. Liu for SEM observations, Dr. Q. Li and Mr. J.C. Peng for TEM observations. This work was financially supported by National Basic Research Program of China (No. 2006CB605001), National Science Foundation of China (NSFC) under Grant No. 50974148, Shanghai Science and Technology Commission (No. 09DZ1100103).

References

[1] M. Thuvander, K. Stiller, Mater. Sci. Eng. 281A (2000) 96–103.
[2] B.A. Young, X.S. Gao, T.S. Srivatsan, P.J. King, Mater. Des. 28 (2007) 373–379.
[3] R.S. Dutta, R. Tewari, P.K. De, Corros. Sci. 49 (2007) 303–318.
[4] J.J. Kai, G.P. Yu, C.H. Tsai, M.N. Liu, S.C. Yao, Metall. Trans. 20A (1989) 2057–2067.
[5] M.H. Lewis, B. Hattersley, Acta Metall. 13 (1965) 1159–1168.
[6] F.R. Beckitt, B.R. Clark, Acta Metall. 15 (1967) 113–129.
[7] R.A. Carolan, R.G. Faulkner, Acta Metall. 36 (1988) 257–266.
[8] E.A. Trillo, L.E. Murr, J. Mater. Sci. 33 (1998) 1263–1271.
[9] B. Sasmal, Metall. Trans. 30A (1999) 2791–2801.
[10] H.U. Hong, B.S. Rho, S.W. Nam, Mater. Sci. Eng. 318A (2001) 285–292.
[11] K. Stiller, J.O. Nilsson, K. Norring, Metall. Mater. Trans. 27A (1996) 327–341.
[12] T.M. Angeliu, G.S. Was, Metall. Trans. 21A (1990) 2097–2107.
[13] Q. Li, B.X. Zhou, Acta Metall. Sin. (Chin. Lett.) 37 (2001) 8–12.
[14] Y.S. Lim, J.S. Kim, H.P. Kim, H.D. Cho, J. Nucl. Mater. 335 (2004) 108–114.
[15] G. Sui, J.M. Titchmarsh, G.B. Heys, J. Congleton, Corros. Sci. 39 (1997) 565–587.
[16] S.M. Bruemmer, C.H. Henager Jr., Scr. Metall. 20 (1986) 909–914.
[17] E.L. Hall, C.L. Briant, Metall. Trans. 15A (1984) 793–811.
[18] K.S. Min, S.W. Nam, J. Nucl. Mater. 322 (2003) 91–97.
[19] S. Spigarelli, M. Cabibbo, E. Evangelista, G. Palumbo, Mater. Sci. Eng. 352A (2003) 93–99.
[20] L. Schafer, J. Nucl. Mater. 258–263 (1998) 1336–1339.
[21] E.A. Trillo, L.E. Murr, Acta Mater. 47 (1999) 235–245.
[22] M. Kurban, U. Erb, K.T. Aust, Scr. Mater. 54 (2006) 1053–1058.
[23] Y. Zhou, K.T. Aust, U. Erb, G. Palumbo, Scr. Mater. 45 (1) (2001) 49–54.
[24] B. Alexandreanu, B. Capell, G.S. Was, Mater. Sci. Eng. 300A (1–2) (2001) 94–104.
[25] S. Xia, B.X. Zhou, W.J. Chen, W.G. Wang, Scr. Mater. 54 (2006) 2019–2022.
[26] S. Xia, B.X. Zhou, W.J. Chen, J. Mater. Sci. 43 (2008) 2990–3000.
[27] S. Xia, B.X. Zhou, W.J. Chen, Metall. Mater. Trans. 40A (2009) 3016–3030.
[28] G. Palumbo, K.T. Aust, E.M. Lehockey, Scr. Mater. 38 (1998) 1685–1690.
[29] H. Li, S. Xia, B.X. Zhou, J.S. Ni, W.J. Chen, Acta Metall. Sin. (Chin. Lett.) 45 (2009) 195–198.
[30] S. Downey II, P.N. Kalu, K. Han, Mater. Sci. Eng. 480A (2008) 96–100.
[31] L.K. Singhal, J.W. Martin, Acta Metall. 15 (1967) 1603–1610.